Conformational and Redox Equilibria and Dynamics of Cytochrome *c* Immobilized on Electrodes via Hydrophobic Interactions

Laura Rivas,[†] Daniel H. Murgida,[†] and Peter Hildebrandt*[,†]

Max-Planck-Institut für Strahlenchemie, Stiftstr. 34-36, D-45470 Mülheim, Germany

Received: November 14, 2001; In Final Form: January 28, 2002

Surface enhanced resonance Raman (SERR) spectroscopy was employed to study structure and dynamics of cytochrome *c* (Cyt-*c*) immobilized on Ag electrodes that were coated with self-assembled monolayers (SAM) of *n*-alkanethiols $HS-(CH_2)_n-CH_3$. Cyt-*c* is bound to these electrodes by hydrophobic interactions most likely via the peptide segment 81−85 that may partially penetrate into the monolayers. The immobilized proteins are partially converted to the conformational state B2 that exhibits a different heme pocket structure and coordination configuration than the native state B1. The B2/B1 conformational equilibrium, which can also be induced by binding to electrodes coated with ω-carboxyl alkanethiols (Murgida, D. H.; Hildebrandt, P. *J. Phys. Chem. B* **2001**, *105*, 1578), is potential-dependent with the B1 state prevailing at potentials < -0.3 V. On hydrophobic coatings, the equilibrium constant is largely independent of the thickness of the SAM except for $HS-CH_2CH_3$ coatings, which do not allow integration of the apolar peptide segment. Using time-resolved SERR spectroscopy, the dynamics of the conversion from the ferric B2 state to the ferrous B1 state were analyzed. The underlying conformational transitions are potential-dependent and involve a fast step (ca. 10^4-10^5 s^{-1}) that may either be the formation of the ferric B2 state or the back-conversion to the ferrous B1 state. The conformational transitions are substantially faster than those observed for electrostatically bound Cyt-*c* where rearrangements of the hydrogen-bonding network in the protein are associated with high electric field induced activation barriers. For the hydrophobically bound Cyt-*c*, the fast conformational transitions proceed on the same time scale as the intermolecular electron transfer between Cyt-*c* and its natural partner cytochrome *c* oxidase and may play a role in the biological process.

I. Introduction

It is well established that electrostatic interactions play a crucial role for binding of cytochrome *c* (Cyt-*c*) to its natural reaction partners cytochrome *c* oxidase (CcO), cytochrome *c* reductase, and cytochrome *c* peroxidase.[1] These interactions involve several lysine residues on the front surface of Cyt-*c* that form a ring-like pattern around the exposed heme edge and match the arrangements of negative charges on the binding domains of the partner proteins. Previous studies have shown that charge neutralization at the positions of these lysines either by chemical modification or by site-directed mutagenesis may substantially reduce the enzymatic activity of the partner proteins toward Cyt-*c*.[2] Thus, it was concluded that the specific arrangement of complementary charges in the protein−protein interface is essential for a proper alignment of the proteins in the reactive complex such that their redox centers are oriented in a way that is most favorable for the intermolecular electron transfer (ET).

In addition, it was found that changes in the maximum reaction rate that is derived from steady-state enzyme kinetics correlate with the portion of the conformational state B2 of Cyt-*c* formed upon binding to CcO.[3] This conformational state differs from the native form of Cyt-*c* (denoted as B1) by structural changes in the heme pocket including the heme coordination pattern and, hence, exhibits quite different electron-transferring properties.[4] Therefore, the involvement of these lysine residues in the interactions with CcO is obviously also important for inducing functionally relevant structurally changes in Cyt-*c*. Qualitatively, the same structural changes are observed when Cyt-*c* binds to anionic surfaces that exhibit a largely uniform distribution of negative charges such as phospholipid vesicles, micelles, polyanions, and electrodes.[3−6] In view of these findings and on the basis of various studies on Cyt-*c*/lipid interactions,[7−9] Coulombic forces can be considered to represent the dominant mode of interaction of Cyt-*c* with its reaction partners as well as with biological membranes.

On the other hand, specifically at high ionic strength and low surface pressure, Cyt-*c* is capable to penetrate partially into phospholipid bilayers implying that hydrophobic interactions are involved.[7,10] Furthermore, amphiphilic molecules such as sodium dodecyl sulfate can bind to Cyt-*c* even without substantial changes of the protein secondary structure.[11] In both cases, however, structural changes in the heme pocket are induced that are spectroscopically indistinguishable from those in electrostatically stabilized complexes.[5] Therefore, hydrophobic interactions are also obviously important for binding of Cyt-*c* to biological membranes, specifically for penetration of the bilayer. This latter process takes place when Cyt-*c* is transferred from the inner mitochondrial space to the cytosol where the protein participates in reaction cascades of apoptosis.[12] Also for Cyt-*c*'s original ET function in the respiratory chain, hydrophobic interactions cannot be ruled out. Site-directed mutagenesis studies of CcO from *Paracoccus denitrificans* have demonstrated that Trp-121 is essential for complex formation with Cyt-*c*,[13] which in turn implies the involvement of hydro-

[†] Present address: Instituto de Tecnologia Química e Biológica, Apartado 127, Av. da República, 2781−901 Oeiras, Portugal.

* To whom correspondence should be addressed. Tel.: +351 21 446 9741. Fax: +351 21 441 1277. E-mail: hildebrandt@itqb.unl.pt.

10.1021/jp014175m CCC: $22.00
Published on Web 04/17/2002

phobic residues of Cyt-*c*. Thus, elucidation of the consequences of electrostatic and hydrophobic interactions on the structure and ET properties of Cyt-*c* is a prerequisite for understanding the mechanism of its biological function on a molecular level.

Our previous studies were focused on the analysis of the conformational and redox equilibria and dynamics of Cyt-*c* under the influence of electrostatic interactions. In these experiments, Cyt-*c* was immobilized on Ag electrodes that were either coated with specifically adsorbed anions or self-assembled monolayers of carboxyl-terminated alkanethiols.[14,15,16a] Such devices allow employing surface enhanced resonance Raman (SERR) spectroscopy, which selectively probes the vibrational spectrum of the heme solely of the bound Cyt-*c* and, thus, provides information about its redox site structures.[14−17] On the basis of potential-dependent stationary and time-resolved SERR spectroscopic experiments, equilibria and kinetics of the various interfacial processes could be analyzed.[14,15,17] Specifically, these studies demonstrate that upon increasing electrostatic field, the conformational equilibrium B2/B1 is shifted toward state B2 and the heterogeneous ET process is slowed drastically compared to Cyt-*c* in solution.[14]

In the present work, we have extended this approach to Cyt-*c* immobilized on Ag electrodes with hydrophobic coatings that were obtained by self-assembly of *n*-alkanethiols ($HS-(CH_2)_n-CH_3$). The goals of this study are (i) to determine the structural changes of the bound Cyt-*c* that are induced by hydrophobic interactions, (ii) to characterize the potential-dependence of the conformational equilibria, and (iii) to analyze the dynamics of the conformational transitions and the ET process.

II. Materials and Methods

Chemicals. Ethanethiol ($HS-CH_2-CH_3$), *n*-pentanethiol ($HS-(CH_2)_4-CH_3$), *n*-dodecanethiol ($HS-(CH_2)_{11}-CH_3$), *n*-octadecanethiol ($HS-(CH_2)_{17}-CH_3$), dimyristoylphosphatidyl glycerol (DMPG), and palmitic acid (PA) were purchased from Sigma and were used without further purification. Cyt-*c* (horse heart) was obtained from Sigma and was purified as previously published.[18]

Preparation of Coated Electrodes. SAMs were produced by spontaneous chemisorption upon dipping the electrochemically roughened silver electrodes into 1 mM solutions of alkanethiols [$HS-(CH_2)_n-CH_3$, $n = 1, 4, 11, 17$] in ethanol for 24 h. The samples were subsequently rinsed by a copious amount of ethanol to remove all the unbound material and were dried under a stream of nitrogen. SAM coatings of ω-carboxyl alkanethiols (i.e., $HS(CH_2)_{10}COOH$) were prepared in a similar way.

SERR Experiments. SERR spectra were measured at ambient temperature with the 413-nm excitation line of a Kr^+-laser (Coherent Innova 302) using a spectrograph (U1000, ISA) equipped with a liquid nitrogen cooled CCD camera. The spectral resolution was 4 cm^{-1} and the step width (increment per data point) was 0.53 cm^{-1}. Details of the experimental setup are given elsewhere.[17] The laser beam (ca. 60 mW) was focused onto the surface of a rotating Ag electrode. The SAM-modified Ag electrode was placed into the electrochemical cell containing the supporting electrolyte (12.5 mM potassium phosphate buffer (pH = 7) and 12.5 mM K_2SO_4) and 0.1 μM Cyt-*c*, which was allowed to adsorb at −0.044V versus saturated calomel electrode (SCE). The electrochemical cell and the protocol for SER activation of the electrode is described elsewhere.[14,17] All potentials cited in this work refer to the saturated calomel electrode.

Time-resolved SERR experiments were carried out by applying a potential jump and probing the relaxation process by SERR spectroscopy after a delay time δ during a measuring interval Δt. A description of the experimental setup as well as of the principles of the time-resolved experiments is given elsewhere.[14,19]

Stationary and time-resolved SERR spectra were analyzed quantitatively by fitting the component spectra of the individual species to the measured spectra according to the procedure reported by Döpner et al.[20]

III. Results

In the spectral region between 1300 and 1650 cm^{-1}, SERR and RR spectra of heme proteins display a characteristic vibrational signature of the oxidation, spin, and coordination state of the heme. Thus, this region is particularly appropriate for identifying Cyt-*c* species that differ with respect to their heme structure. In fact, for various conformational states of ferric and ferrous Cyt-*c*, previous RR and SERR studies have provided component spectra, which constitute a sound basis for the quantitative analysis of conformational equilibria and dynamics in the present work.[5,17]

Electrostatic and Hydrophobic Binding of Cyt-*c* to SAM-Coated Electrodes. When a Ag electrode coated with a $HS-(CH_2)_{10}-COOH$ monolayer is placed into a solution of 0.2 μM Cyt-*c*, the protein is adsorbed electrostatically via interactions with the carboxylate headgroups. Under these conditions, the SERR spectrum measured at −0.044 V displays a prominent band at 1360 cm^{-1} with a distinctly weaker shoulder at 1373 cm^{-1}, both located in the ν_4-mode region. These bands are indicative for a ferrous and a ferric heme, respectively.[21] A careful spectra analysis reveals that these species correspond to the oxidized and reduced six-coordinated low spin (6cLS) forms of the native Cyt-*c*, denoted as B1, whereas no other conformational states of Cyt-*c* contribute to the SERR spectrum.[17] In the potential range from +0.1 to −0.45 V, potential-dependent measurements have been used to determine the redox potential of the state B1, yielding −0.031 V for Cyt-*c* immobilized on $HS-(CH_2)_{10}-COOH$/SAM.[17] Thus, the SERR spectrum in Figure 1A (−0.044 V) reflects a concentration ratio of ferric and ferrous B1 of approximately 1.7:1.

Replacing the $HS-(CH_2)_{10}-COOH$/SAM coated Ag electrode by an electrode covered with a $HS-(CH_2)_{11}-CH_3$ monolayer, the SERR spectrum obtained under otherwise identical conditions displays pronounced differences in band intensities and frequencies (Figure 1B). Specifically, the band at ca. 1360 cm^{-1} has disappeared, implying that the contribution from the reduced Cyt-*c* is very small. Thus, the 1490 cm^{-1} band in the ν_3-mode region must largely result from a ferric five-coordinated high spin (5cHS) configuration as it is observed when Cyt-*c* binds to anionic surfaces such as liposomes, SDS micelles, or electrodes at high electrostatic fields.[5,17,19,22] Under these conditions, Cyt-*c* is converted to a conformational state B2, in which the native axial Met-80 ligand is removed from the heme to yield either a 5cHS configuration or, upon coordination by a water molecule or His-33, a six-coordinated high spin (6cHS) or 6cLS configuration, respectively.[4] Compared to the ferric B1 form, this 6cLS species of B2, that is the prevailing form in complexes with SDS micelles (Figure 1C), exhibits a distinctly lower ν_{10} intensity and higher ν_3 and ν_{10} frequencies, which in turn agrees very well with the SERR spectrum of Cyt-*c* bound to the $HS-(CH_2)_{11}-CH_3$/SAM Ag electrode (Figure 1B). Thus, the visual inspection of the SERR spectra already suggests that

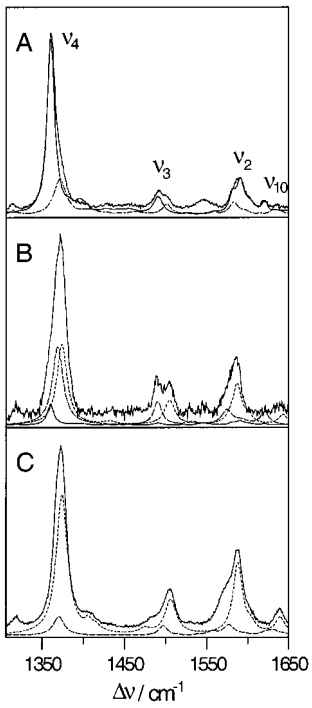

Figure 1. SERR spectra of Cyt-*c* in the marker band region between 1300 and 1650 cm^{-1} adsorbed at −0.044 V on a (A) HS−$(CH_2)_{10}$–COOH coated Ag electrode, and a (B) HS−$(CH_2)_{11}CH_3$ coated Ag electrode, compared with (C) the RR spectrum of ferric Cyt-*c* in aqueous solution (pH 7.0) containing 10 mM SDS. The component spectra of the various species are indicated by different line types. $B1_{red}$: −; $B1_{ox}$: −•−; $B2_{ox}$(6cLS): ••••••••••; $B2_{ox}$(5cHS): -----.

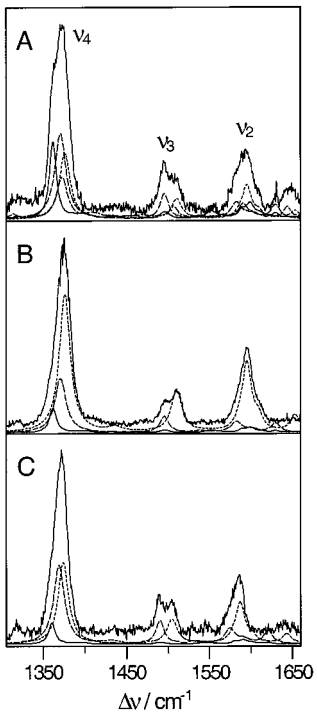

Figure 2. SERR spectra of Cyt-*c* hydrophobically adsorbed on Ag electrodes coated with (A) HS−CH_2–CH_3, (B) HS−$(CH_2)_4$–CH_3, and (C) HS−$(CH_2)_{11}$–CH_3. The component spectra of the various species are indicated by different line types. $B1_{red}$: −; $B1_{ox}$: −•−; $B2_{ox}$(6cLS): ••••••••••; $B2_{ox}$(5cHS):-----.

upon binding to the hydrophobic monolayer of the electrode, the conformational state B2 is formed. In fact, this conclusion is confirmed by the component analysis, demonstrating that the 5cHS and 6cLS forms of the B2 state are the main components whereas the contribution of the native ferrous B1 state is very small. The oxidized B1 state is not detectable at all.

The SERR experiments were extended to Cyt-*c* bound to (HS−$(CH_2)_n$−CH_3), n = 1, 4, 17, coated electrodes. Whereas for (HS−$(CH_2)_{17}$–CH_3) and (HS−$(CH_2)_{11}$–CH_3) coatings, nearly identical SERR spectra were obtained; the contribution of the 5cHS species of state B2 is lower in the SERR spectrum measured from a (HS−$(CH_2)_4$–CH_3) coated electrode at −0.044 V (Figure 2C, B). Substantial differences are noted for the (HS−CH_2–CH_3) coated electrode inasmuch as the portion of reduced B1 is distinctly higher than for the other coatings as reflected by the pronounced 1360 cm^{-1} shoulder of the ν_4-envelope (Figure 2A). Furthermore, in the latter spectrum even a substantial contribution of the oxidized B1 is found as indicated by the relatively high intensity in the ν_{10}-mode region at ca. 1635 cm^{-1}. Regardless of the qualitative differences between these spectra, the overall SERR intensity for Cyt-*c* bound to the hydrophobic surfaces displays a much weaker distance-dependence as compared to Cyt-*c* electrostatically adsorbed on carboxyl-terminated SAMs with different alkyl chain lengths.[17]

Potential-Dependent Equilibria of Cyt-*c*. The potential-dependent distribution among the various species was studied for Cyt-*c* bound to (HS−$(CH_2)_n$−CH_3) coated electrodes (n = 1, 4, 11, 17) by measuring the SERR spectra in the potential range between 0.056 and −0.444 V. A selection of such spectra obtained from a (HS−$(CH_2)_4$–CH_3) coated Ag electrode is shown in Figure 3. The component analysis demonstrates that with decreasing potential the portion of the reduced B1 increases at the expense of the oxidized B2, specifically of the 6cLS form,

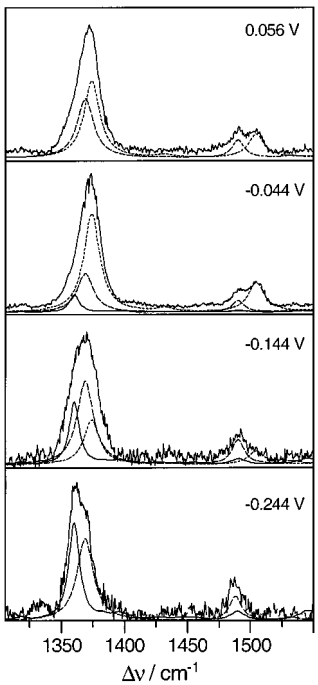

Figure 3. SERR spectra of Cyt-*c* on HS−$(CH_2)_4$–CH_3 coated Ag electrodes at different potentials. The component spectra of the various species are indicated by different line types. $B1_{red}$: −; $B1_{ox}$: −•−; $B2_{ox}$(6cLS): ••••••••••; $B2_{ox}$(5cHS):-------.

such that the reduced B1 becomes the prevailing species at −0.444 V. With increasingly negative potential (i.e., E < −0.194 V), the overall SERR intensity decreases accompanied by a broadening of the bands. At E < −0.444 V, the spectral quality is too poor for a reliable spectra analysis and the loss of SERR intensity is irreversible, that is, upon setting the potential back to positive values the original intensity is not recovered.

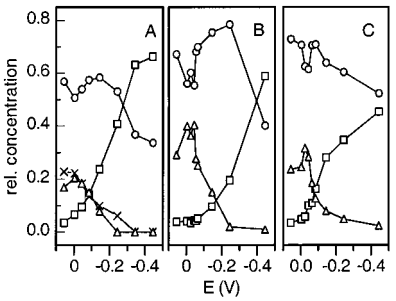

Figure 4. Potential-dependent distributions among the various species of Cyt-*c* immobilized on electrodes coated with SAMs of (A) HS−(CH_2)−CH_3, (B) HS−$(CH_2)_4$−CH_3, and (C) HS−$(CH_2)_{11}$−CH_3. The relative concentrations of the various species are represented by the following symbols: $B1_{red}$: □; $B1_{ox}$: X; $B2_{ox}$(6cLS): △; $B2_{ox}$(5cHS): ○.

Applying the component analysis,[20] the SERR spectra were simulated by a set of component spectra of the B1 and B2 states to obtain the various relative spectral contributions, which were subsequently converted into relative concentrations (Figure 4). The component spectra of the individual species as well as their relative reciprocal scattering cross sections were adopted from previous studies.[5,17,19] Good global fits were obtained solely on the basis of the component spectra of four species, that is, the oxidized and reduced B1 as well as the oxidized 5cHS and 6cLS species of B2. No contributions from the reduced B2 and the oxidized 6cHS form of B2 were detectable for any of the hydrophobically coated electrodes. For the (HS−$(CH_2)_{17}$−CH_3) coated electrode (data not shown), essentially the same potential-dependent distribution among the various Cyt-*c* species was found as for the (HS−$(CH_2)_{11}$−CH_3) coated electrode.

In all cases, the contribution of the 6cLS form of B2 cannot be detected anymore at potentials < -0.344 V, whereas there is still a considerable portion of the 5cHS even at -0.444 V. A complete conversion to the reduced B1 state appears to occur only at potentials lower than -0.544 V. However, already at potentials below -0.444 V, a reliable analysis of the SERR spectra is not possible anymore because of the irreversible loss of SERR intensity. This effect is attributed to the destruction of the SAM structure that causes desorption of the protein. In fact, Boubour et al. have reported a transformation of the monolayer structure of *n*-alkanethiol SAMs below a critical potential, which on Au electrodes was determined to be between -0.35 V and -0.15 V depending on the alkyl chain length.[23]

The potential-dependent distribution of the 5cHS form of B2 displays a minimum at ca. -0.044 V which is observed for all coatings regardless of the chain length. The analysis of the redox equilibria is restricted to the B1 state on the HS−CH_2−CH_3 coated electrode, which is the only device where both oxidation states of a redox couple are detectable. A Nernstian plot (not shown) reveals a very good linear correlation with an apparent redox potential of $E^\circ = -0.084$ V and $n = 0.35$.

Time-Resolved SERR Experiments. To determine the dynamics of the conformational transitions and ET kinetics, time-resolved (TR) SERR experiments were carried out with Cyt-*c* on (HS−$(CH_2)_4$−CH_3) coated Ag electrodes by employing potential jumps from the initial potential $E_i = -0.044$ V to final potentials E_f of -0.144 V and -0.194 V. All TR SERR spectra could be satisfactorily simulated solely by the component spectra of the reduced B1 and the oxidized 5cHS and 6cLS forms of B2. No contribution of the oxidized B1 or the reduced B2 states was detectable at any delay time. A selection of TR SERR spectra obtained at various delay times δ is shown in Figure 5

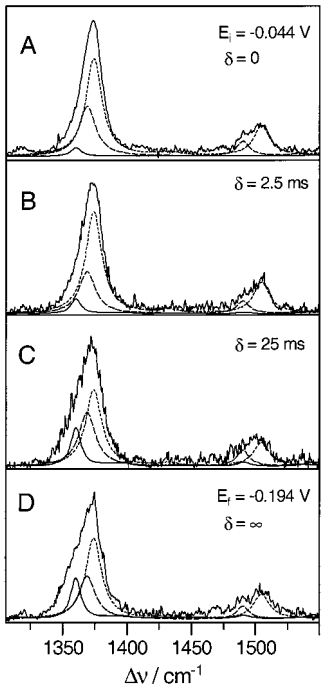

Figure 5. Stationary and time-resolved SERR spectra of Cyt-*c* on a HS−$(CH_2)_4$−CH_3 coated Ag electrodes. (A), stationary SERR spectrum ($\delta = 0$) at $E_i = -0.044$ V; (B), (C), time-resolved SERR spectra measured after different delay times δ following the potential jump from $E_i = -0.044$ V to $E_f = -0.194$ V; (D) stationary SERR spectrum at $E_f = -0.194$ V. The component spectra of the various species are indicated by different line types. $B1_{red}$: −; $B1_{ox}$: −·−; $B2_{ox}$(6cLS): ·····; $B2_{ox}$(5cHS):-------.

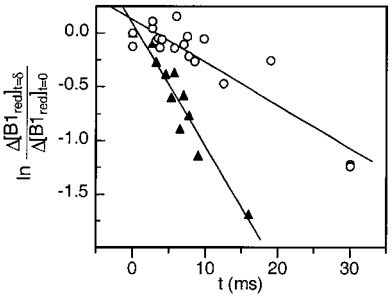

Figure 6. Semilogarithmic plots of the concentration changes of $B1_{red}$ as a function of δ as determined from the time-resolved SERR spectra. $\Delta C(\delta)$ and $\Delta C(t_0)$ denote the deviations from the equilibrium concentrations for E_f at $t = \delta$ and $t = 0$. The open circles and solid triangles refer to the results obtained from potential jump experiments with $E_f = -0.144$ V and $E_f = -0.194$ V, respectively.

along with the stationary SERR spectra at $E_i = -0.044$ V and $E_f = -0.194$ V. It can clearly be seen that already after 2.5 ms, the portion of the reduced B1 has increased considerably while it has nearly reached its equilibrium value after 25 ms. The increase of the reduced B1 is accompanied by a decrease of the oxidized 6cLS form of B2 whereas the relative contribution of the corresponding 5cHS species appears to remain largely unchanged. The time-dependent concentration changes of the reduced B1, as derived from the quantitative analysis of the TR SERR spectra, are plotted in Figure 6 in a semi-logarithmical manner, leading to a relaxation time of $\tau = 9$ ms at -0.194 V, which is substantially faster than for the potential jump to $E_f = -0.144$ V ($\tau = 24$ ms). An even shorter relaxation time of less than 1 ms can be estimated from preliminary experiments for a potential jump to $E_f = -0.444$ V.

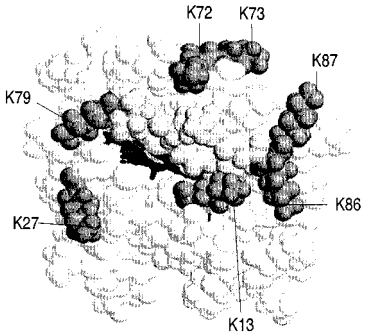

Figure 7. Front view of the structure of ferric Cyt-*c*. The heme is shown in black, lysine residues in dark gray, and hydrophobic residues in light gray.

IV. Discussion

Immobilization of Cytochrome *c* via Electrostatic and Hydrophobic Interactions. Cyt-*c* exhibits a high molecular dipole moment with the positive end of the vector located at the exposed heme edge on the front surface of the protein.[24] This region includes various positively charged lysine residues surrounding the heme edge (Figure 7). Hence, upon approaching a negatively charged surface as, for instance, provided by an electrode coated with a *ω*-carboxyl alkanethiols SAM, the protein is likely to orient itself with this lysine-rich domain pointing to the anionic headgroups of the monolayer and to form an electrostatic complex. At least seven lysine residues may be involved in electrostatic binding such that, in principle, Cyt-*c* may adopt slightly different (sub-) orientations as concluded from a previous analysis of the electron-transfer dynamics.[15]

Until recently, electrostatic interactions were thought to be a prerequisite for the formation of the conformational state B2 inasmuch as it has been detected upon Cyt-*c* binding to a variety of negatively charged surfaces including phospholipid vesicles, polyanions, and electrodes covered with specifically adsorbed anions ("bare" electrodes).[6,19,22] The conversion to state B2 at first requires the rupture of the Fe−Met-80 bond (5cHS) and, at least for a portion of the Cyt-*c* molecules, binding of His-33 or His-26 (6cLS).[4] This process may be primarily due to structural perturbations of the heme pocket that are initiated by formation of intermolecular salt bridges between various lysine residues in the binding domain of Cyt-*c* and the negatively charged groups of the anionic surface. Furthermore, upon immobilization of Cyt-*c* on electrodes with anionic coatings at low protein coverage, state B2 is only formed on $HS-(CH_2)_x-COOH$/SAMs with $x < 11$ and its portion increases with decreasing alkyl chain length, that is, with increasing electric field strength.[17] Thus, there is obviously also a long-range electric field effect, originating from interfacial potential drops, that influences the conformational equilibria of the adsorbed protein in addition to the localized ion−ion interactions.

The SAM-coated electrodes used in the present study do not exhibit negatively charged headgroups so that binding of Cyt-*c* must occur via hydrophobic interactions. On the first sight, it is surprising that hydrophobic binding of this highly cationic protein is so efficient as indicated by the relatively high SERR intensity. At positive potentials, the SERR intensity is of the same order of magnitude as observed for electrostatically bound Cyt-*c* under otherwise identical conditions, pointing to comparably large binding constants for electrostatic and hydrophobic immobilization of the oxidized protein. The SERR signals cannot be attributed to Cyt-*c* molecules that are directly adsorbed on the Ag electrode because of possible imperfections of the monolayers. For SAMs with carboxylate headgroups, such imperfections cannot account for more than 0.5% of the measured SERR intensity.[17] This conclusion should also hold for hydrophobic coatings particularly since destabilization of these SAMs that may occur upon lowering the potential is accompanied by a decrease rather than an increase of the SERR intensity (vide infra).

Inspection of the protein surface of Cyt-*c* reveals a hydrophobic patch including I85, G84, A83, F82, and I81 that may serve as the interaction domain for binding to apolar SAMs. Also, this peptide segment is located close to the exposed heme edge, that is, in the center of the ring constituted by the lysine residues involved in electrostatic binding (Figure 7). Thus, the gross orientation of the protein is likely to be quite similar upon electrostatic and hydrophobic binding.

Cyt-*c* does not bind to SAMs of hydroxyl-terminated alkanethiols.[17] Unlike to apolar SAMs, Cyt-*c* immobilization on these surfaces is not associated with a gain in entropy because of a reduction of the solvent-exposed hydrophobic area. Furthermore, hydroxyl groups are not capable to form sufficiently strong hydrogen bonds with charged or polar residues on the protein surface.

Hydrophobic interactions lead to the same structural changes of the heme as observed in electrostatic complexes since the corresponding RR and SERR are indistinguishable and reflect the formation of the 5cHS and 6cLS species of B2.[5] However, the conformational transition is induced via a mechanism different to that in electrostatic complexes since different amino acids are involved in immobilization. The peptide segment implicated in hydrophobic binding is directly linked to the Met-80 ligand, which has to be dissociated from the heme iron in the first step of the B1 → B2 conversion. A displacement of this segment away from the heme pocket would inevitably weaken and eventually break the Fe−Met bond. Moreover, this movement increases the exposure and accessibility of these amino acids so that the effective contact area for hydrophobic interactions is enlarged, which in turn may be essential for Cyt-*c* immobilization via hydrophobic forces. It may well be that this peptide segment penetrates to some extent into the hydrophobic SAM in analogy to the partial integration of Cyt-*c* into liposomes.[7,10] Such an interpretation is consistent with the experimental observations made in the present study.

The B2/B1 concentration ratio is approximately the same for $HS-(CH_2)_{11}-CH_3$ and $HS-(CH_2)_{17}-CH_3$ coatings with a value of ca. 15 in the potential range between +0.05 and −0.05 V and is only slightly lower for $HS-(CH_2)_4-CH_3$ coatings. However, the ratio is substantially decreased to ca. 4 at the $HS-CH_2-CH_3$ coated electrode where even a partial penetration of apolar amino acids can be ruled out. These findings suggest that integration of the hydrophobic peptide segment into the monolayers is important albeit not essential for the formation of B2. Conversely, long chain lengths ($HS-(CH_2)_{11}-CH_3$, $HS-(CH_2)_{17}-CH_3$) would allow integration of a relatively large fraction of this peptide segment and possibly even further hydrophobic parts of the protein including the heme itself. In this case, the distance of the heme with respect to the electrode may become actually shorter than for Cyt-*c* immobilized on the anionic surfaces of electrodes coated with *ω*-carboxyl alkanethiols. This interpretation may also account for the observation that the drop of SERR intensity with the alkanethiols chain length is less pronounced than for anionic SAMs.

Redox and Conformational Equilibria. For $HS-(CH_2)_4-CH_3$, $HS-(CH_2)_{11}-CH_3$, and $HS-(CH_2)_{17}-CH_3$ coatings, the only species that are detectable by SERR spectroscopy in the potential range from +0.05 to −0.45 V are the 6cLS and 5cHS

forms of the oxidized state B2 and the reduced state B1. The potential-dependence of the relative concentrations of the various species (Figure 4) indicates that with decreasing potential the portion of the reduced B1 steadily increases at the expense of the oxidized B2. Whereas for HS−$(CH_2)_{17}$–CH_3 and HS−$(CH_2)_{11}$–CH_3 coatings, essentially the same potential-dependent distribution among the various species is observed, the B1 content is slightly lower for HS−$(CH_2)_4$–CH_3 in the potential range between −0.1 and −0.25 V. It may be that at closer proximity to the electrode, the electric field, generated by the interfacial potential drop, further stabilizes state B2. Since the field strength decreases with decreasing potential, the portion of B1 increases at potentials < −0.25 V so that the B2/B1 ratio becomes similar to that for longer chain lengths.

The structural changes in B2 are associated with a drastic decrease of the redox potential from +0.01 V (B1) to −0.375 and −0.425 V for the 5cHS and 6cLS redox couples of B2, respectively, as determined for Cyt-*c* adsorbed on bare Ag electrodes.[4] Thus, one would expect that upon lowering the potential, the 5cHS species is reduced prior to the 6cLS form. However, the opposite behavior is observed and, moreover, the appreciable portion of the oxidized 5cHS species even at −0.544 V points to a significant negative shift of the redox potential. Such a negative potential shift cannot be attributed to an interfacial potential drop because of the lack of anionic groups in the SAM/Cyt-*c* interface. Conversely, a hydrophobic environment may cause even a positive shift of the redox potentials, which, in fact, may hold for all redox couples.[10d] Thus, it is concluded that the 5cHS species reflects a state in which additional protein structural changes have occurred that lower the reducibility of the heme.

The conformational state B2 has been characterized in detail by various spectroscopic methods. In electrostatic complexes of Cyt-*c*, the reversible structural changes compared to the native state primarily refer to the heme pocket, and the ligand exchange is not associated with alterations of the secondary structure.[4,5] However, for the B2 state of Cyt-*c* adsorbed on bare electrodes, there are indications for further structural changes particularly at very high electric fields (i.e., positive potentials) that are quasi-irreversible since back-conversion to the native state B1 is very slow.[25] As these conversions are not accompanied by changes in the SERR spectra, the underlying conformational changes are likely to include rearrangements of the protein structure. In view of the results of the present work, we conclude that upon hydrophobic binding of Cyt-*c*, similar extended protein structural changes occur. These changes do not notably affect the heme structure since the SERR spectrum of the 5cHS species is identical to that reversibly formed upon electrostatic binding to liposomes or SDS micelles.[5] The B2 state of ferric Cyt-*c*, induced by hydrophobic interactions with SDS monomers, exclusively exists in the 6cLS configuration that exhibits a RR spectrum indistinguishable from the RR and SERR spectra of the corresponding species in electrostatic complexes (Figure 1). As SDS binding causes only a moderate loss of the secondary structure,[5] it may be that the 5cHS species of Cyt-*c* immobilized on hydrophobic SAMs reflects a largely unfolded state of the protein. This interpretation can also account for the results obtained in the present time-resolved SERR experiments inasmuch as the ferric 5cHS species is not involved in the relaxation process (vide infra).

Consequently, the reversible potential-dependent processes of the hydrophobically bound Cyt-*c* may adequately be described by the reaction scheme in Figure 8, where $B2_{ox}$ and $B2_{red}$ exclusively refer to the 6cLS species.

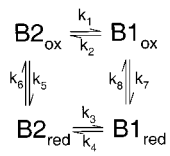

Figure 8. Reaction scheme for the coupled conformational and redox equilibria of immobilized Cyt-*c*.

On HS−CH_2–CH_3 coatings, the potential-dependent redox and conformational equilibria of Cyt-*c* display a different behavior. Since this monolayer does not allow integration even of a small peptide segment, binding may not only occur via the amino acids 81−85 but also via other regions on the protein surface. In the latter case, hydrophobic interactions do not necessarily lead to structural changes in the heme pocket so that its native structure may be preserved. This interpretation can account for the substantially higher contribution of B1 (oxidized and reduced) as compared to Cyt-*c* adsorbed on SAMs of longer chain lengths. Furthermore, it is consistent with the analysis of the B1 redox equilibrium. The value of $n = 0.35$ and the distinct negative shift of the apparent redox potential to −0.084 V that are determined from the Nernstian plot are indicative for a substantial heterogeneity in the orientation of the bound Cyt-*c* which would be the consequence of different binding sites.[26]

Dynamics of Conformational Transitions and Electron-Transfer Kinetics. The potential jump experiments were carried out with HS−$(CH_2)_4$–CH_3 SAMs where the orientation of the immobilized Cyt-*c* can be considered to be largely uniform (vide supra). Then the minimum reaction model for the relaxation processes is given by the scheme in Figure 8 where $B2_{ox}$ exclusively refers to the 6cLS configuration since the 5cHS species was constant on the time scale of the experiments. The conversion from $B2_{ox}$ to $B1_{red}$ may occur via two pathways, that is, via $B1_{ox}$ or $B2_{red}$. These two species are not detectable either in the stationary SERR spectra at the initial or final potential or in the time-resolved SERR spectra at any delay time. Thus, steady-state approximations are justified for $B1_{ox}$ and $B2_{red}$, that is, $d[\Delta B1_{ox}]/dt \approx 0$ and $d[\Delta B2_{red}]/dt \approx 0$. Then the relaxation of $B1_{red}$ follows a monoexponential decay

$$-\frac{d[\Delta B1_{red}]}{dt} = \tau^{-1} \tag{1}$$

with the reciprocal relaxation time $1/\tau$ given by

$$\tau^{-1} = \frac{(k_1k_7 + k_2k_8)(k_3 + k_6) + (k_3k_5 + k_4k_6)(k_2 + k_7)}{(k_3 + k_6)(k_2 + k_7)} \tag{2}$$

where the rate constants are defined in Figure 8.

The heterogeneous ET reaction of B1 (k_7, k_8) has been studied previously, revealing a normal (exponential) distance dependence in the absence of an electrostatic barrier.[14] This condition is also fulfilled for Cyt-*c* immobilized on the hydrophobic HS−$(CH_2)_4$–CH_3/SAM coating where the redox site of the protein is separated from the electrode by approximately 10 Å. Then, the formal ET rate constants (at a driving force of zero electronvolts) is estimated to be larger than 10^7 s^{-1} on the basis of the pre-exponential factor and electron tunneling parameter determined previously.[14] Taking into account the redox potential E° for B1 of +0.01 V,[17,27] the potential jump experiments with $E_f = -0.144$ V and −0.194 V are associated with driving forces for the reduction of B1 (k_7) of −0.15 and −0.2 eV, respectively. For the B2 (6cLS) redox couple, the redox potential was

determined to be −0.425 V,[4] so that the driving forces for the B2 oxidation (k_6) are −0.23 and −0.28 eV for $E_f = -0.194$ and −0.144 V, respectively. Thus, although the formal heterogeneous ET rate constant of B2 (6cLS) is not known, a value of 10^7 s^{-1} can safely be considered as the lower limit for the rate constants k_6 and k_7.

So far, the kinetics of the conformational transitions have only been determined for the conversion from the $B1_{ox}$ to $B2_{ox}$ (6cLS) of Cyt-*c* bound to SDS micelles and was found to occur in the millisecond range.[5] Under denaturing conditions in guanidinium hydrochloride solution, conformational transitions of Cyt-*c* that involve the replacement of Met-80 by His-33 (His-26) occur with rate constants that do not exceed 10^3 s^{-1}.[28] Thus, it is very likely that the ET steps are faster than the conformational transitions $B1_{ox} \rightarrow B2_{ox}$ (k_2) and $B2_{red} \rightarrow B1_{red}$ (k_3), that is, $k_7 \gg k_2$ and $k_6 \gg k_3$. Then eq 2 simplifies to

$$\tau^{-1} = k_1 + k_2\frac{k_8}{k_7} + k_4 + k_3\frac{k_5}{k_6} \tag{3}$$

Using the conformational and redox equilibrium constants

$$K_C(\text{ox}) = \frac{[B2_{ox}]}{[B1_{ox}]} = \frac{k_2}{k_1} \tag{4}$$

$$K_C(\text{red}) = \frac{[B2_{red}]}{[B1_{red}]} = \frac{k_4}{k_3} \tag{5}$$

$$K_R(B1) = \frac{[B1_{red}]}{[B1_{ox}]} = \frac{k_7}{k_8} = \exp\left(-\frac{nF(E - E^0_{B1})}{RT}\right) \tag{6}$$

$$K_R(B2) = \frac{[B2_{red}]}{[B2_{ox}]} = \frac{k_5}{k_6} = \exp\left(-\frac{nF(E - E^0_{B2})}{RT}\right) \tag{7}$$

where *F*, *R*, and *T* have the usual meaning ($n = 1$), one obtains

$$\tau^{-1} = k_1\frac{(1 + C)}{C} + k_4(1 + C) \tag{8}$$

with *C* expressed by

$$C = \frac{K_R(B1)}{K_C(\text{ox})} = \frac{K_R(B2)}{K_C(\text{red})} = \frac{[B1_{red}]}{[B2_{ox}]} \tag{9}$$

The values for *C*, that is the ratio of the equilibrium concentrations of $B1_{red}$ and $B2_{ox}$, can be derived from the stationary SERR spectra measured at the final potentials. Then, the only unknown parameters in eq 8 are the rate constants for the conformational transitions from $B2_{ox}$ to $B1_{ox}$ (k_1) and $B1_{red}$ to $B2_{red}$ (k_4).

Assuming that one of these conformational transitions is negligibly slow, an upper limit for the rate constant of the respective transition can readily be evaluated. For $E_f = -0.144$ V, these limits are 7.5 s^{-1} and 33 s^{-1} for k_1 and k_4, respectively, whereas for $E_f = -0.194$ V, $k_1 = 25$ s^{-1} and $k_4 = 90$ s^{-1} are obtained. These values allow calculating the upper limits for the respective back reaction rate constants (k_2, k_3) according to eq 8 (Table 1). The determination of k_2 and k_3 depends on the redox potentials of B1 and B2, which for the present estimation are assumed to be the same as those obtained from the SERR spectroscopic analysis of Cyt-*c* adsorbed on electrodes via electrostatic interactions. It cannot be ruled out that the immobilization on the hydrophobic SAM causes a positive shift of the redox potentials (vide supra),[27] which in turn would lead to an increase of k_2 and a decrease of k_3.

TABLE 1: Equilibrium Constants and Upper Limits for the Rate Constants of the Conformational Transitions of Cyt-*c* Immobilized on $HS-(CH_2)_4-CH_3$ coated Ag Electrodes[a]

		$B2_{ox} \rightarrow B1_{red}$ via $B1_{ox}$			$B2_{ox} \rightarrow B1_{red}$ via $B2_{red}$		
E_f/V	τ^{-1}/s^{-1}	k_1/s^{-1}	K_2/s^{-1}	K_C(ox)	k_4/s^{-1}	k_3/s^{-1}	K_C(red)
−0.144	41	7.5	$1.45\cdot10^4$	$1.9\cdot10^3$	33	$5.2\cdot10^5$	$6.4\cdot10^{-5}$
−0.194	114	25	$3.0\cdot10^5$	$1.2\cdot10^4$	90	$2.3\cdot10^5$	$4.0\cdot10^{-4}$

[a] Rate and equilibrium constants are defined in Figure 8 and by eqs 4 and 5.

In any case, the present results indicate that the conformational transitions of Cyt-*c* must involve fast steps that occur within less than 100 microseconds, that is, either the formation of B2 in the ferric state or the back-conversion to B1 in the reduced state or both. At present, it is not possible to decide which of these conformational transitions represents the preferred pathway from $B2_{ox}$ to $B1_{red}$.[29]

Fast conformational transitions appear to be a specific property of Cyt-*c* immobilized on hydrophobic SAMs. At least, the formation of $B2_{ox}$ is obviously much slower for Cyt-*c* electrostatically bound to electrodes or SDS micelles, where k_2 has been determined to be ca. between 100 and 10 s^{-1}.[5,19] Since these conformational transitions involve a rearrangement of the hydrogen-bonding network, the rate of the underlying proton transfer steps may be substantially reduced in the presence of strong electrostatic fields. Such an effect has been recently observed for the reorganization of the heme pocket structure associated with ET.[14] Conversely, hydrophobic interactions do not impose such constraints either on the conformational transitions or on ET, which, hence, are much faster than for electrostatically immobilized Cyt-*c*.

Previous studies have shown that the conformational state B2 is also formed in the fully oxidized complex between Cyt-*c* and CcO, although the kinetics of the conformational transitions have not yet been determined.[3] Formation of the protein complex is not only achieved via electrostatic forces but also involves hydrophobic interactions.[2,13] Therefore, it may well be that the electrostatic fields experienced by Cyt-*c* bound to CcO are weaker than upon immobilization on anionic SAMs. Consequently, the conformational dynamics of Cyt-*c* in the complex with CcO may occur on the same time scale as for the hydrophobically bound protein. In that case, conformational transitions are likely to proceed within the lifetime of the Cyt-*c*/CcO complex, which under physiological conditions is about a few milliseconds.[30] Specifically, the $B1_{ox} \rightarrow B2_{ox}$ transition could be of functional relevance. Taking into account that the redox potentials of Cyt-*c* in state B1 and of the primary electron acceptor of CcO (Cu_A) are very similar[31] and the intramolecular ET from Cu_A to heme *a* is estimated to be four times slower than the intermolecular ET from Cyt-*c* to Cu_A (ca. 60000 s^{-1}),[32] unproductive back ET to Cyt-*c* is unavoidable. This reaction, however, can be blocked if, after the ET to Cu_A, Cyt-*c* (i.e., $B1_{ox}$) is converted to $B2_{ox}$ for which this back ET reaction is very slow because of the low redox potential (−0.4 V). Hence, this coupling of the ET with a conformational transition may guarantee the unidirectionality of the redox process.

Conclusions

1. Cyt-*c* can be immobilized to electrodes coated with hydrophobic SAMs via the peptide segment 81−85 which may partially penetrate the monolayers. The driving force for Cyt-*c*

binding is most likely the reduction of the solvent-exposed hydrophobic area, which leads to an entropy gain.

2. The hydrophobic interactions induce the formation of the conformational state B2, which exhibits the same heme structure as observed for electrostatically bound Cyt-*c*.

3. As compared to electrostatically immobilized Cyt-*c*, the rate constants for conformational transitions are much larger when Cyt-*c* binds via hydrophobic interactions. The rates of the fastest steps, that are $B2_{red} \rightarrow B1_{red}$ or $B1_{ox} \rightarrow B2_{ox}$, are of the same order of magnitude as the ET from Cyt-*c* to CcO and, hence, may control the electron flow in this step of the respiratory chain.

Acknowledgment. The work was supported by the Deutsche Forschungsgemeinschaft (Hi 464/4-2). The authors wish to thank Professor D. Möbius for valuable discussions and comments on the manuscript.

References and Notes

(1) Pettigrew, G. W.; Moore, G. R. *Cytochrome c*- Biological Aspects, Springer-Verlag. Berlin, 1987.

(2) (a) Smith, H. T.; Staudenmayer, N.; Millet, F. *Biochemistry* **1977**, *16*, 4971. (b) Speck, S. H.; Fergunson-Miller, S.; Osheroff, N.; Margoliash, E. *Proc. Natl. Acad. Sci. U.S.A.* **1979**, *76*, 55. (c) Rieder, R.; Bosshard H. R. *J. Biol. Chem.* **1980**, *255*, 4732.

(3) Döpner, S.; Hildebrandt, P.; Rosell, F. I.; Mauk, A. G.; von Walter, M.; Soulimane, T.; Buse, G. *Eur. J. Biochem.* **1999**, *261*, 379.

(4) Wackerbarth, H.; Murgida, D. H.; Oellerich, S.; Döpner, S.; Rivas, L.; Hildebrandt, P. *J. Mol. Struct.* **2001**, *563*−*564*, 51.

(5) Oellerich, S. Ph.D. Thesis, Universität GH Essen/Max-Planck-Institut für Strahlenchemie, 2001.

(6) Hildebrandt, P. *Biochim. Biophys. Acta* **1990**, *1040*, 175.

(7) Peschke, J.; Möhwald, H. *Colloids Surf.* **1987**, *27*, 305.

(8) Kozarac, Z.; Dhathatthreyan, A.; Möbius, D. *FEBS Lett.* **1987**, *229*, 372.

(9) Jordi, W.; de Kruiff, B. In *Cytochrome c* − *A Multidisciplinary Approach*; Scott, R. A., Mauk, A. G., Eds.; University Science Books: Sausalito, CA, 1995; p 449.

(10) (a) Cortese J. D.; Voglino, A. L.; Hackenbrock, C. R. *Biochim. Biophys. Acta* **1995**, *1228*, 216. (b) Heimburg, T.; Marsh, D. *Biophys. J.* **1995**, *68*, 536. (c) Rytömaa, M.; Kinnumen, P. K. J. *J. Biol. Chem.* **1995**, *270*, 3197. (d) Salamon, Z.; Tollin, G. *J. Bioenerg. Biomembr.* **1997**, *29*, 211.

(11) Das, T. K.; Shyamalava, M.; Mitra, S. *Eur. J. Biochem.* **1998**, *254*, 662.

(12) (a) Green, D. R. *Cell* **1998**, *94*, 695. (b) Hengartner, M. O. *Nature* **2000**, *407*, 770. (c) Jemmerson, R.; Liu, J.; Hausauer, D.; Lam, K. P.; Mondino, A.; Nelson, R. D. *Biochemistry* **1999**, *39*, 8234.

(13) Witt, H.; Malatesta, F.; Nicoletti, F.; Brunori, M.; Ludwig, B. *J. Biol. Chem.* **1998**, *273*, 5132.

(14) Murgida, D. H.; Hildebrandt, P. *J. Am. Chem. Soc.* **2001**, *123*, 4026.

(15) Murgida, D. H.; Hildebrandt, P. *Angew. Chem., Int. Ed.* **2001**, *40*, 728.

(16) (a) Hildebrandt, P.; Stockburger, M. *Biochemistry* **1989**, *28*, 6710. (b) Hobara, D.; Niki, K.; Cotton, T. M. *Biospectroscopy* **1998**, *4*, 161. (c) Dick, L. A.; Kaes, A. J.; van Duyne, R. P. *J. Phys. Chem. B.* **2000**, *104*, 11752.

(17) Murgida, D. H.; Hildebrandt, P. *J. Phys. Chem. B* **2001**, *105*, 1578.

(18) Brautigan, D. L.; Feinberg, B. B.; Hoffman, B. M.; Margoliash, E.; Peisach, J.; Blumberg, W. E. *J. Biol. Chem.* **1977**, *252*, 574.

(19) Wackerbarth, H.; Klar, U.; Günther, W.; Hildebrandt, P. *Appl. Spectrosc.* **1999**, *53*, 283.

(20) Döpner, S.; Hildebrandt, P.; Mauk, G. A.; Lenk, H.; Stempfle, W. *Spectrochim. Acta, Part A* **1996**, *51*, 573.

(21) Parthasarathi, N.; Hansen, C.; Yamaguchis, S.; Spiro, T. G. *J. Am. Chem. Soc.* **1987**, *113*, 3865.

(22) Hildebrandt, P.; Heimburg, T.; Marsh, D. *Eur. Biophys. J.* **1990**, *18*, 193.

(23) Boubour, E.; Lennox, R. B. *J. Phys. Chem. B.* **2000**, *104*, 9004.

(24) Koppenol, W. H.; Rush, J. D.; Mills, J. D.; Margoliash, E. *Mol. Biol. Evol.* **1991**, *8*, 545.

(25) Wackerbarth, H. Ph.D. Thesis, Universität GH Essen/Max-Planck-Institut für Strahlenchemie, 2000.

(26) Murgida, D. H.; Hildebrandt, P. *J. Mol. Struct.* **2001**, *565*−*566*, 97.

(27) A redox potential of +0.01 V is considered to be the lower limit since otherwise the oxidized form of state B1 should be detectable in the SERR spectra measured at potentials >0.0 V (cf. Figure 3).

(28) Yeh, S. R.; Han, S. W.; Rousseau, D. L. *Acc. Chem. Res.* **1998**, *31*, 727.

(29) Since the native B1 state is much more stable in the ferrous than in the ferric form, it is likely that k_1 is larger than k_4.

(30) Soulimane, T.; Buse, G. *Eur. J. Biochem.* **1995**, *227*, 588.

(31) Malatesta, F.; Antonini, G.; Sarti, P.; Brunori, M. *Biophys. Chem.* **1995**, *54*, 1.

(32) Geren, L. M.; Beasley, B. R.; Fine, B. R.; Saunders, A. J.; Hibdon, S.; Pielak, G. J.; Durham, B.; Millet, F. *J. Biol. Chem.* **1995**, *270*, 2466.